QUANTUM INFORMATION

Electrical and optical control of single spins integrated in scalable semiconductor devices

Christopher P. Anderson[1,2]*, Alexandre Bourassa[1]*, Kevin C. Miao[1], Gary Wolfowicz[1], Peter J. Mintun[1], Alexander L. Crook[1,2], Hiroshi Abe[3], Jawad Ul Hassan[4], Nguyen T. Son[4], Takeshi Ohshima[3], David D. Awschalom[1,2,5]†

Spin defects in silicon carbide have the advantage of exceptional electron spin coherence combined with a near-infrared spin-photon interface, all in a material amenable to modern semiconductor fabrication. Leveraging these advantages, we integrated highly coherent single neutral divacancy spins in commercially available p-i-n structures and fabricated diodes to modulate the local electrical environment of the defects. These devices enable deterministic charge-state control and broad Stark-shift tuning exceeding 850 gigahertz. We show that charge depletion results in a narrowing of the optical linewidths by more than 50-fold, approaching the lifetime limit. These results demonstrate a method for mitigating the ubiquitous problem of spectral diffusion in solid-state emitters by engineering the electrical environment while using classical semiconductor devices to control scalable, spin-based quantum systems.

Solid-state defects have enabled many proof-of-principle quantum technologies in quantum sensing (*1*), computation (*2*), and communications (*3*). These defects exhibit atom-like transitions that have been used to generate spin-photon entanglement and high-fidelity single-shot readout (*4*), enabling demonstrations of long-distance quantum teleportation, entanglement distillation, and loophole-free tests of Bell's inequalities (*3*). However, fluctuating electric fields and uncontrolled charge dynamics have limited many of these technologies (*1*, *4*–*7*). For example, lack of charge stability and of photon indistinguishability are major problems that reduce entanglement rates and fidelities in quantum communication experiments (*4*–*6*). In particular, indistinguishable and spectrally narrow photon emission is required to achieve high-contrast Hong-Ou-Mandel interference (*8*). This indistinguishability has been achieved with some quantum emitters through dc Stark tuning the optical lines into mutual resonance (*9*, *10*). A variety of strategies (*1*, *6*, *11*–*13*) have also been proposed to reduce spectral diffusion (*14*) and blinking (*15*), but consistently achieving narrow and photostable spectral lines remains an outstanding challenge (*16*). In addition, studies of charge dynamics (*17*, *18*) have enabled quantum-sensing improvements (*1*, *7*) and spin-to-charge conversion (*19*), allowing electrical readout of single-spin defects (*20*). However, these experiments have largely been realized in materials such as diamond, in which scalable nanofabrication and doping techniques are difficult to achieve.

By contrast, the neutral divacancy (VV^0) defect in silicon carbide (SiC) presents itself as a candidate spin qubit in a technologically mature host, allowing for flexible fabrication, doping control, and availability on the wafer scale. These defects display many attractive properties, including all-optical spin initialization and readout (*21*), long coherence times (*22*), nuclear spin control (*23*), as well as a near-infrared high-fidelity spin-photon interface (*24*). However, VV^0 has displayed relatively broad optical lines (*24*), charge instability (*18*), and relatively small Stark shifts (*10*). Furthermore, the promise of integration into classical semiconducting devices remains largely unexplored.

Here, we use the mature semiconductor technology that SiC provides to create a p-i-n structure that allows tuning of the electric field and charge environment of the defect. First, we isolate and perform high-fidelity control on highly coherent single spins in the device. We then show that these devices enable wide dc Stark tuning while maintaining defect symmetry. We also demonstrate that charge depletion in the device mitigates spectral diffusion, thus greatly narrowing the linewidths in the optical fine structure. Finally, we use this device as a testbed to study the photoionization dynamics of single VV^0, resulting in a method for deterministic optical control of the defect charge state.

The effects presented here suggest that doped SiC structures are flexible and scalable quantum platforms hosting long-lived, single-spin qubits with an electrically tunable, high-quality optical interface. The demonstrated reduction in electric field noise can lead to increased spin coherence (*25*) and electrical tuning of "dark" spins in quantum sensing (*26*), whereas charge control could extend the memory time of nuclear spins (*27*). Additionally, this platform opens new avenues for spin-to-charge conversion, electrically driven single-photon emission (*28*), electrical control (*29*), and readout (*20*, *30*, *31*) of single spins in SiC CMOS (complementary metal oxide semiconductor)-compatible and optoelectronic semiconductor devices.

Isolated single defects in a semiconductor device

We first isolated and controlled single VV^0 in a 4H-SiC p-i-n diode created through commercial growth of doped SiC epilayers. After growth, we electron irradiated and annealed our samples to create single, isolated VV^0 defects. We fabricated microwave striplines and ohmic contact pads, allowing for spin manipulation and electrical gating (Fig. 1A) (*32*). In contrast to other defects in SiC, such as the isolated silicon vacancy (*33*), the divacancy is stable above 1600°C (*34*), making it compatible with device processing and high-temperature annealing to form ohmic contacts.

Spatial photoluminescence (PL) scans of the device showed isolated emitters corresponding to single VV^0 (Fig. 1B), as confirmed by second-order correlation ($g^{(2)}$) measurements (Fig. 1B, inset) (*32*). The location in depth of the observed defects is consistent with isolation to the i-type layer. This is to be expected because formation energy calculations (*35*) indicate that the neutral charge state is energetically favorable when the Fermi level is between ~1.1 and 2 eV, and this condition must be satisfied somewhere in the i-type layer (*32*, *36*). This depth localization provides an alternative to delta doping (*37*), which is not possible with intrinsic defects, facilitating positioning and control in fabricated devices (fig. S1). Additionally, owing to the diode's highly rectifying behavior at low temperature, large reverse biases are possible with low current (Fig. 1C) (*32*).

Sweeping the frequency of a narrow-line laser, we obtained photoluminescence excitation (PLE) spectra of the optical fine structure of these single defects (Fig. 1D). Using the observed transitions for resonant readout and preparation, we performed high-contrast Rabi oscillations of isolated VV^0 in the p-i-n structure (Fig. 1E) (*32*). The contrast exceeded 98%, improving on previous demonstrations through the use of resonant spin polarization (*24*). Additionally, a single-spin Hahn-echo decay time of 1.0 ± 0.1 ms was measured for spins in the device (Fig. 1F), consistent with previous ensemble measurements (*22*). The long Hahn-echo times and high-fidelity control demonstrate that integration into the semiconductor structures does not degrade the spin properties of VV^0. This isolation and control of highly coherent spin qubits achieved

[1]Pritzker School of Molecular Engineering, University of Chicago, Chicago, IL 60637, USA. [2]Department of Physics, University of Chicago, Chicago, IL 60637, USA. [3]National Institutes for Quantum and Radiological Science and Technology, 1233 Watanuki, Takasaki, Gunma 370-1292, Japan. [4]Department of Physics, Chemistry and Biology, Linköping University, SE-581 83 Linköping, Sweden. [5]Center for Molecular Engineering and Materials Science Division, Argonne National Laboratory, Lemont, IL 60439, USA.
*These authors contributed equally to this work.
†Corresponding author. Email: awsch@uchicago.edu

in these functioning semiconductor devices unlocks the potential for integration with a wide range of classical electronic technologies.

Large Stark shifts in a p-i-n diode

Because the (*hh*) and (*kk*) divacancies (*32*) in SiC are nominally symmetric along the c-axis (growth axis), the geometry of the diode allows for large electric fields that mostly conserve the symmetry of the defect. Therefore, wide tuning of the VV^0 optical structure is possible while reducing unwanted mixing from transverse or symmetry-breaking components of the excited-state Hamiltonian (*9*, *24*, *38*). Because the i-type region can be relatively thin (10 μm here), the applied voltage is dropped over a much smaller region than if a bulk sample were used (*10*), leading to significantly larger Stark shifts for a given applied voltage. In principle, this region can be reduced to a thickness that exceeds limitations from optical access with metal planar gates (limited by the optical spot size of ~1 μm). Furthermore, it is possible to use doped layers as in situ transparent native contacts to Stark tune and control localized defects in suspended photonic or phononic structures (*39*), enabling complex hybrid electrical, photonic, and phononic devices.

In our p-i-n junction device, we applied up to 420 V in reverse bias. Our results show Stark tuning of several hundreds of gigahertz on different defects of the same type and on inequivalent lattice sites, where the Stark shift was between 0.4 and 3.5 GHz/V after a threshold was passed (Fig. 2A). For example, we observed a (*hh*) divacancy shifted by >850 GHz (2.5 meV) at a reverse bias of 420 V and a (*kh*) divacancy shifted by >760 GHz at a reverse bias of 210 V (Fig. 2B). These shifts are among the largest reported for any single-spin defect to date and were only limited by the voltage output of our source. We expect that, owing to the high dielectric breakdown field of SiC, even higher shifts of a few terahertz are possible (*32*). The high-field limit of these shifts corresponds to estimated dipole moments ($d_{||}$) of 11 GHz m/MV and 4.5 GHz m/MV for (*hh*) and (*kk*) divacancies, respectively, consistent with previous reports (*10*, *40*). For the (*kh*) basal divacancy observed, the estimated transverse dipole moment is $d_{\perp} \sim 35$ GHz m/MV. Furthermore, because the Stark shift represents a measure of the local electric field, we conclude that negligible field is applied to the VV^0 before a certain threshold voltage where the depletion region reaches the defect (*41*). This results from nonuniform electric fields in the diode caused by residual n-type dopants in the intrinsic region [Fig. 2C (*32*)].

Overall, our system could be used as a widely frequency-tunable, spectrally narrow source of single photons. In particular, our system enables one of the highest Stark shift-to-linewidth ratios (>40,000) obtained in any solid-state single-photon source (table S1). These characteristics make this system ideally suited for tuning remote defects into mutual resonance and for frequency multiplexing of entanglement channels (*42*). The tunability range is so wide that it could even enable the tuning of a (*hh*) divacancy into resonance with a (*kk*) divacancy, allowing for interference and entanglement between different species of defects. This wide tunability stems from the rectification behavior of the diode, which allows large electric fields without driving appreciable currents that can degrade spin and optical properties. Furthermore, the observed sensitivity of the optical structure of single VV^0 defects could serve as a nanoscale

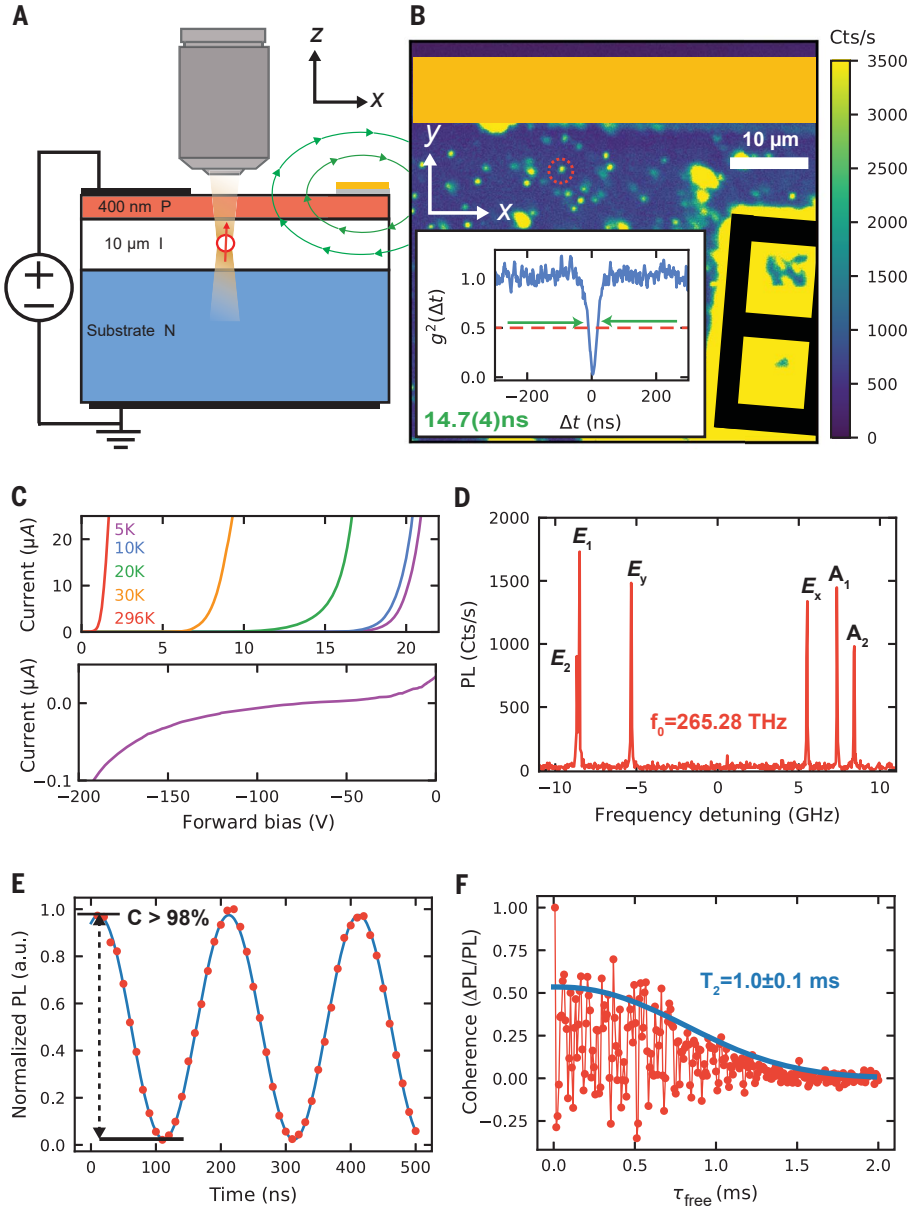

Fig. 1. Isolation of single VV^0 in a commercially grown semiconductor device. (**A**) Schematic of the device geometry. (**B**) Spatial PL scan of an example device showing isolated emitters (example circled in red) confirmed by autocorrelation (inset) showing $g^{(2)}$ (0) < 0.5 (red line). Extracted emitter lifetime is 14.7 ± 0.4 ns (green arrows). Gate and microwave stripline features are drawn and color coded as in (A). Cts, counts. (**C**) Top: Current–voltage (*I*–*V*) curves of the device at various temperatures; bottom: low-temperature reverse bias behavior. C, contrast. (**D**) PLE spectrum of a single (*kk*) divacancy at 270 V of reverse bias. (**E**) Optically detected Rabi oscillations of a single (*kk*) VV^0 with >98% contrast (fit in blue) using resonant initialization and readout. a.u., arbitrary units. (**F**) Hahn-echo decay of a single (*kk*) VV^0 in the diode. Rabi, Hahn, and $g^{(2)}$ data are taken at 270 V of reverse bias and at ~240 Gauss at T = 5 K.

electric field sensor, enabling field mapping in these working devices with sensitivities of ~100 $(V/m)/\sqrt{Hz}$ or better, which is competitive with state-of-the-art spin- and charge-based electrometry techniques (*32*, *43*–*46*).

Reducing spectral diffusion using charge depletion

Uncontrolled fluctuating electrical environments are a common problem in spin systems, where they can cause dephasing (*25*), as well as in quantum emitters, where they result in spectral diffusion of the optical structure and lead to large, inhomogeneous broadening. For example, adding and removing just a single electron charge 100 nm away causes shifts of

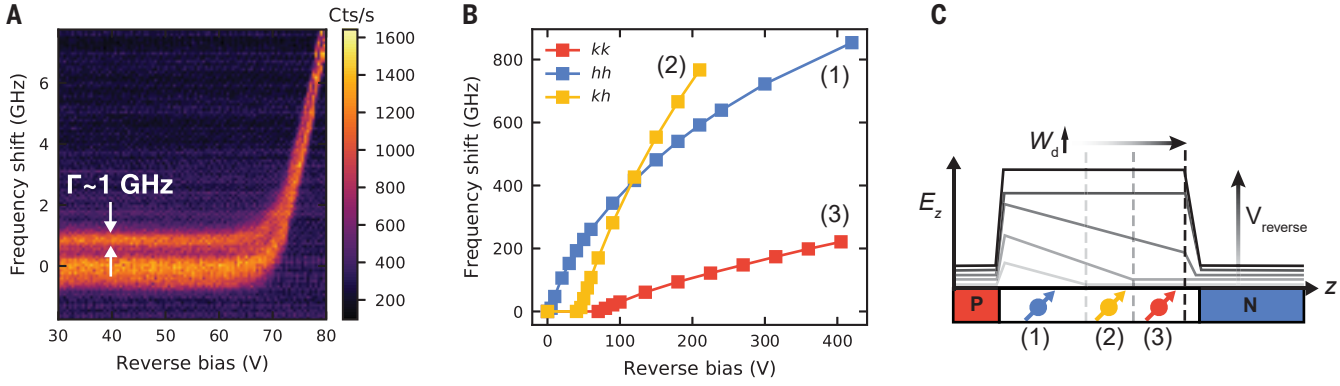

Fig. 2. Stark shifts in p-i-n diode. (**A**) Low-field Stark tuning of a single (*kk*) defect showing a turn-on behavior for the Stark shifts and a narrowing with voltage. This threshold is the same as that in Fig. 4A. These scans contain the lower branch (E_1, E_2, and E_y) where the linewidth of E_y is ~1 GHz and E_1 and E_2 are unresolved. The PLE lines show no shifting down to zero bias. (**B**) High-field Stark shifts of multiple example defects (located at various depths and positions in the junction) showing >100 GHz shifts. (**C**) Schematic electric field distribution and depletion region width (W_d) in the diode for increasing reverse bias. Location in the junction can determine the local field experienced by the defects in (B). The error bars in (B) are smaller than the point size. All data were obtained at T = 5 K.

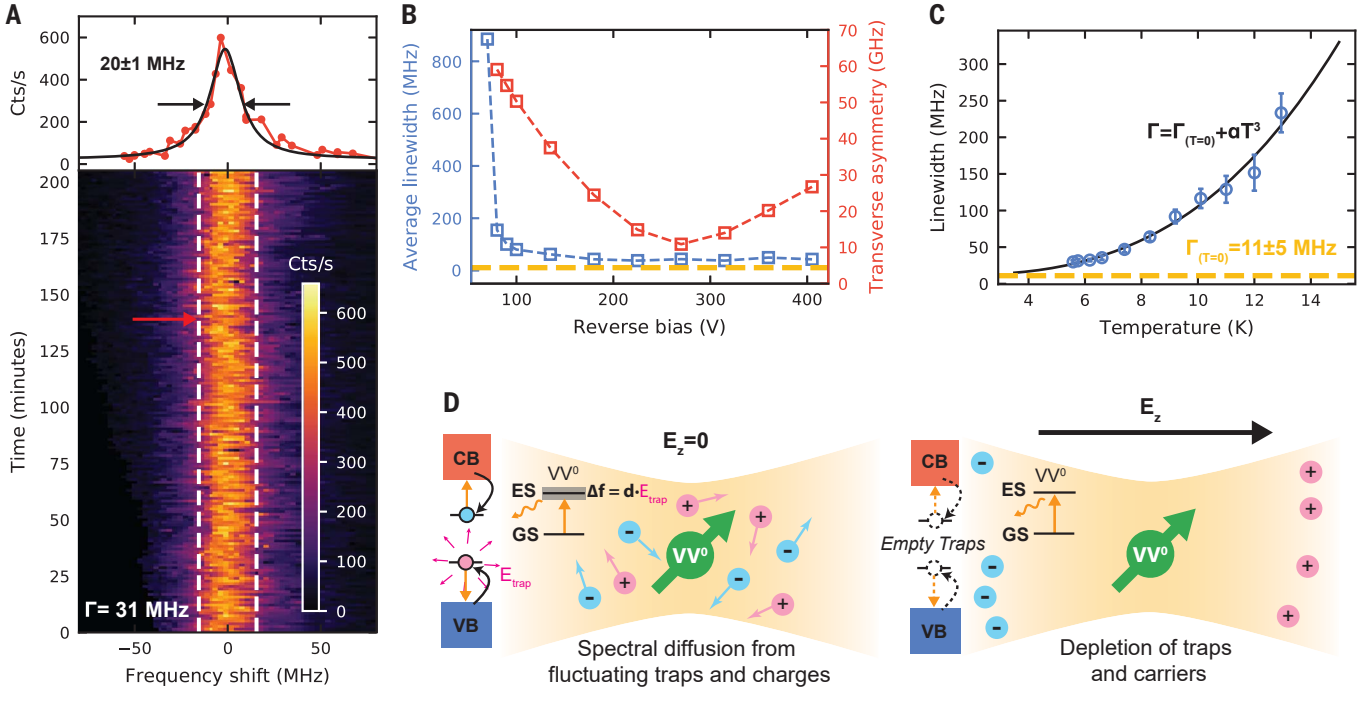

Fig. 3. Optical linewidth narrowing by tuning the electrical environment of a solid-state emitter. (**A**) Multiple PLE sweeps taken over 3.5 hours of the E_x line showing small residual spectral diffusion (fitted inhomogeneous linewidth of 31 ± 0.4 MHz). The red arrow corresponds to the single scan shown with a fitted linewidth of ~20 MHz. (**B**) Comparison of the average linewidth of all orbitals (blue) and defect transverse asymmetry (red) with respect to applied reverse bias. The yellow line is the lifetime limit. (**C**) Temperature dependence of the linewidth. A free power law fit gives an exponent of 3.2 ± 0.3. Constraining the fit to a T^3 relation, we extract a zero temperature linewidth of 11 ± 5 MHz (yellow line). Errors on the plot represent a 95% confidence interval. (**D**) Model for the effect of charge depletion on spectral diffusion in the illuminated volume (yellow). To the left of each diagram is a schematic band diagram with the relevant transitions. CB, conduction band; VB, valence band; GS, ground state; ES, excited state. Errors for the fits values in (A) and (C) represent 1 SD. All data are from a single (*kk*) VV^0. In (B), the laser power is slightly higher than in (A), causing some broadening. For (A) and (C), the E_x line is shown at 270 V of reverse bias. Data in (A) and (B) were obtained at T = 5 K.

~100 MHz for the optical fine structure of VV^0 (fig. S2). Previous work (*24*) has shown that by doing an exhaustive search through many defects in a specially grown material, one can find defects with lines as narrow as 80 MHz (typically 100 to 200 MHz or larger); however, this is still much larger than the Fourier lifetime limit of ~11 MHz (*24*). In bulk intrinsic commercial material, the narrowest linewidths are significantly broadened to 130 to 200 MHz or greater (*24*) (fig. S3). Overall, spectral diffusion has been a notoriously difficult outstanding challenge for nearly all quantum emitters in the solid state.

Here, we introduce a technique for mitigating spectral diffusion. We demonstrate that by applying electric fields in our device, we deplete the charge environment of our defect and obtain single-scan linewidths of 20 ± 1 MHz (Fig. 3A) without the need for an exhaustive search. This reduction in PLE linewidth has a different voltage dependence than the transverse asymmetry in the defect, thus eliminating reduced mixing as a possible mechanism for narrowing (Fig. 3B). The temperature dependence of the linewidth is roughly consistent with a T^3 scaling at these low temperatures (*47*) [fitted exponent 3.2 ± 0.3 and a zero-temperature linewidth of 11 ± 5 MHz (*32*)]. Although the dominant temperature scaling may change at lower temperature, this trend hints at a possible explanation for the remaining broadening and is consistent with a temperature-limited linewidth. Furthermore, the observed line is extremely stable, with a fitted inhomogeneous broadening of 31 ± 0.4 MHz averaged for >3 hours (Fig. 3A). This stability over time, narrowness, tunability, and photostability demonstrates the effectiveness of engineering the charge environment with doped semiconductor structures for creating ideal and indistinguishable quantum emitters.

At zero bias, the linewidth in our samples is much higher than in bulk material (~1 GHz; Fig. 2A). We attribute this to a greater presence of traps and free carriers (under illumination). Thus, in these samples, the observed narrowing corresponds to an improvement in the linewidth by a factor of >50. We speculate that a combination of this charge-depletion technique with lower sample temperatures, a lower-impurity material, and further annealing could enable measurement of consistent transform-limited linewidths (*13*, *48*). This use of charge depletion for creating spectrally narrow optical interfaces (Fig. 3D) could be widely applicable to other experiments in SiC or to other solid-state emitters such as quantum dots (*49*, *50*). Indeed, by applying the same techniques developed here to intrinsic SiC materials, lines as narrow as ~21 MHz have been observed (*40*). Crucially, these results demonstrate that depleting local charge environments can transform a very noisy electric environment into a clean one, turning materials containing unwanted impurities into ideal hosts for quantum emitters.

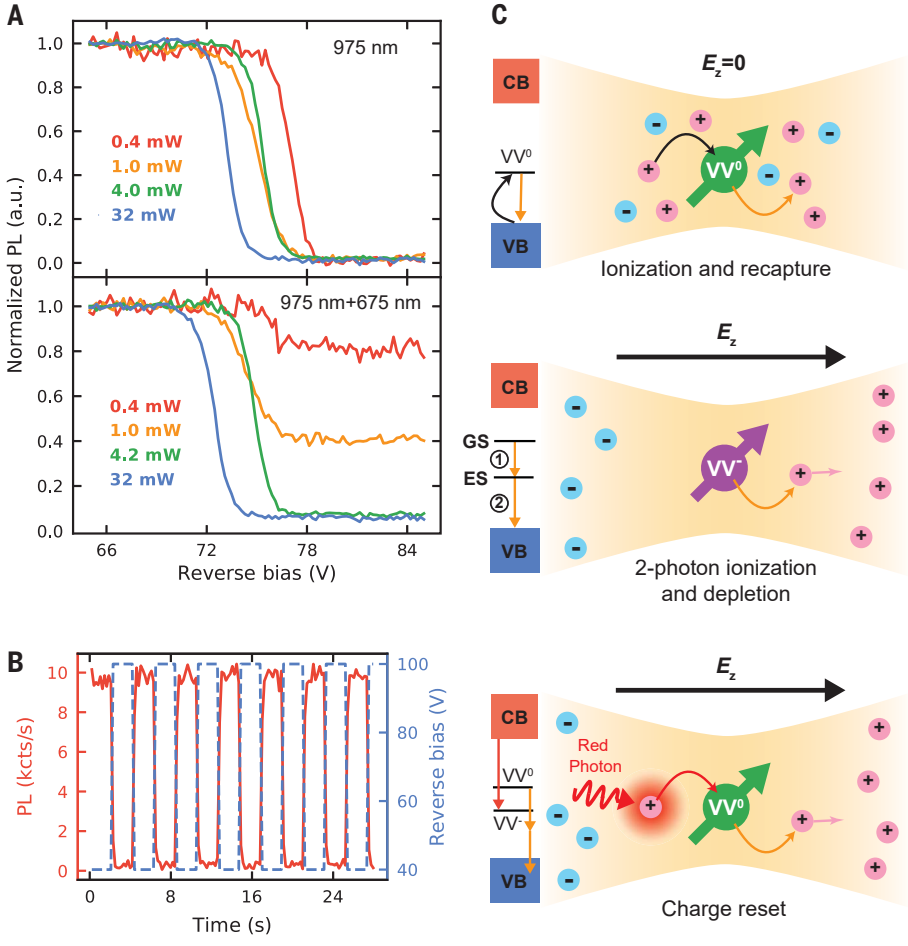

Fig. 4. Electrical and optical charge control of a single VV^0. (**A**) Voltage and power dependence of the photoluminescence of a single (*kk*) VV^0 with 975 nm excitation (top) and with additional 188 μW of 675 nm illumination (bottom), showing a sharp threshold under reverse bias. With high 975-nm power, the two-photon ionization process dominates and the PL signal is low. (**B**) By controlling the voltage in time (blue), the emission from the single (*kk*) defect is switched on and off (red). (**C**) Top: Model of rapid ionization and recapture at zero electric field (top). Middle: Two-photon ionization and formation of a depletion region under reverse bias. Bottom: Charge reset under applied electric field using red light (bottom). All data were obtained at T = 5 K. kcts, kilocounts.

Charge gating and photodynamics of single defects

Our observation of large Stark shifts and linewidth narrowing relies on understanding and controlling charge dynamics under electric fields. To achieve this, we studied the stability of the observed single defects under electrical bias. This allowed a careful investigation of the charge dynamics of single VV^0 under illumination, from which we developed an efficient charge-reset protocol. In our experiments, we observed that with 975 nm off-resonant light, the PL drops substantially once the reverse bias is increased past a threshold voltage (Fig. 4A). This threshold varies between defects, which is expected given differences in the local electric field stemming from variations in position, depth, and local charge-trap density. We attribute the PL reduction to photoionization to an optically "dark" charge state (*18*). We used this effect to create an electrically gated single-photon source (*51*–*53*) in which emission is modulated in time with a gate voltage (Fig. 4B) (*10*). The threshold voltage has a slight hysteresis (fig. S4) and laser power dependence (Fig. 4A), suggesting that trapped charges may play a role (*9*, *54*). The electric field dependence of the photoionization could also be used to extend sensitive electrometry techniques (*46*) to the single-defect regime, and controlled ionization of the spin can extend the coherence of nuclear registers (*27*). The threshold for Stark

shifts (Fig. 2A) corresponds approximately to the same voltage where significant photobleaching occurs when using off-resonant excitation. This links the sharp photoionization threshold in Fig. 4A to the presence of moderate electric fields and the onset of carrier depletion.

A possible explanation for this voltage-dependent PL is that at zero electric field, illumination constantly photoionizes the VV^0 and other nearby traps. However, the divacancy rapidly captures available free carriers, returning it to the neutral charge state. Under applied field, carrier drift depletes the illuminated region of charges. Thus, when a VV^0 photoionization event occurs in this depleted environment, no charges are available for fast recapture, resulting in a long-lived dark state (Fig. 4C).

Past studies have shown that PL is enhanced in ensembles by repumping the charge with higher-energy laser colors (*18*, *55*, *56*). We extended this work to the single-defect regime by applying various illumination energies and studying single-defect photodynamics at 90 V of reverse bias (past the threshold voltage of ~75 V of reverse bias for this defect). We observed under resonant illumination that PL quickly dropped to zero and did not recover, indicating that 1131 nm (1.09 eV) light [resonant with the ZPL of a (*kk*) VV^0] ionizes the defect, but does not reset the charge state. However, after applying higher-energy light (e.g., 688 nm), the charge was returned to a bright state even with <1 nW of applied power. This "repump" of the defect charge state is vital for restoring PL for ionized or charge unstable VV^0 in SiC (Fig. 4A) and is essential to observe the effects discussed in the previous sections (Fig. 4C).

When both near-infrared (NIR) resonant (1131 nm) and red (688 nm, 1.8 eV) light were applied to the defect, alternating between the bright (VV^0) and dark (VV^+ or VV^-) charge states resulted in a blinking behavior. From this blinking (fig. S5), we extract photoionization and repumping rates of the defect (*57*). We first examined the ionization rate of a single VV^0 (Fig. 5A) and observed that the power dependence was quadratic below defect saturation (exponent m = 2.05 ± 0.2) and linear at higher powers (m = 0.99 ± 0.07). Our observed data provide evidence for a two-photon process to VV^- (*32*) suggested in previous ensemble studies (*18*, *56*) and are less consistent with a recently proposed three-photon model converting to VV^+ (*35*, *55*). Thus, we conclude that the dark state caused by NIR resonant excitation is VV^-. Further study of the spin dependence of this ionization may lead to the demonstration of spin-to-charge conversion in VV^0.

Similarly, we studied the charge-reset kinetics by varying the power of the repumping laser. We found a near-linear power law with m = 0.98 ± 0.02 (Fig. 5B). This linear dependence of the repumping rate can be described by two potential models. One possibility is that the dark charge state is directly one-photon ionized by repump laser. The other possible explanation is that nearby traps are photoionized by this color and the freed charges are captured by the divacancy to convert back to the bright state. By varying the color of this reset laser, we found repumping to be most efficient at ~710 nm (1.75 eV), suggesting a particular trap-state energy or a possible defect absorption resonance (*58*, *59*) (Fig. 5C). Overall, we observed negligible ionization from the optimal red repump laser and no observable reset rate from the resonant laser. This results in fully deterministic optical control of the defect charge state [for discussion, see (*32*)], allowing for high-fidelity charge-state initialization for quantum-sensing and communications protocols.

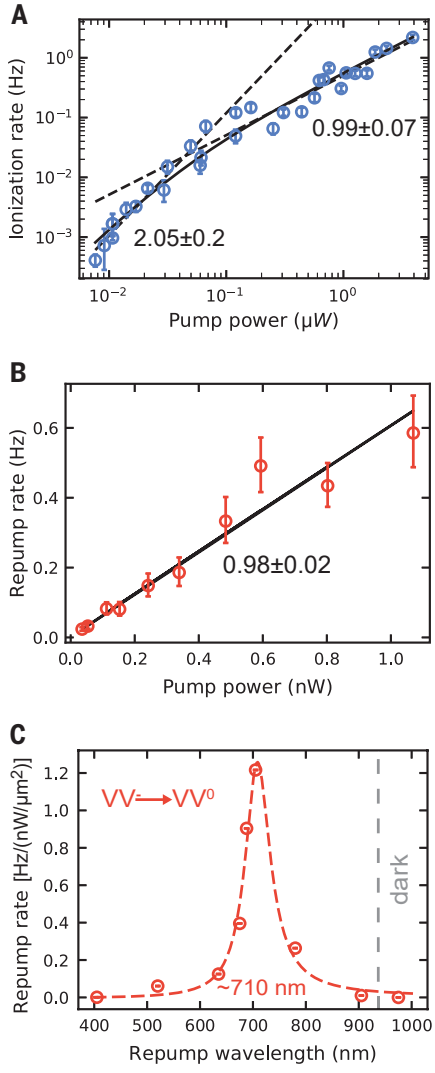

Fig. 5. Ionization and charge reset rates for VV^0. (**A**) Dependence of the ionization rate on resonant laser power. Low- and high-power regime fits (black dotted lines) and their power laws (m = 2.05 ± 0.2 and 0.99 ± 0.07, respectively) are shown. The solid black line shows a full model fit. (**B**) Repump power dependence of the 688 nm laser showing a linear exponent of m = 0.98 ± 0.02. Fluctuations in the polarization or power of the laser limit the true error. (A) and (B) were taken at 90 V of reverse bias. (**C**) Repumping rate as a function of illumination wavelength at 270 V of reverse bias with a Lorentzian fit centered around 710 nm. With wavelengths longer than 905 nm (and at these powers), no PL is observed and the defect is "dark." All error bars represent 95% confidence intervals from the fit of the raw data from a single (*kk*) VV^0. All data were obtained at T = 5 K.

Conclusions and outlook

The electrical tuning of the environment demonstrated here constitutes a general method that could be applicable to various quantum emitters in semiconductors in which spectral diffusion or charge stability is an issue (*60*) or electric field fluctuations limit spin coherence (*25*, *32*). Furthermore, using our p-i-n diode as a testbed to study charge dynamics, we have developed a technique to perform deterministic optical control of the charge state of single divacancies under electric fields (*61*).

The techniques presented here will be vital to achieving single-shot readout and entanglement in VV^0 by enabling charge control and enhancing photon indistinguishability, suggesting doped semiconductor structures as ideal quantum platforms for defects. This work also enables high-sensitivity measurement of nanoscale electric fields and charge distributions in working devices (*43*) and facilitates spin-to-charge conversion (*19*) for enhanced quantum-sensing and electrical readout protocols (*20*). Finally, the introduction of VV^0 into classical SiC semiconductor devices such as diodes, MOSFETs (metal-oxide-semiconductor field-effect transistors), and APDs (avalanche photodiodes), for example, may enable the next generation of quantum devices.

REFERENCES AND NOTES

1. C. Bonato *et al.*, *Nat. Nanotechnol.* **11**, 247–252 (2016).
2. G. Waldherr *et al.*, *Nature* **506**, 204–207 (2014).
3. D. D. Awschalom, R. Hanson, J. Wrachtrup, B. B. Zhou, *Nat. Photonics* **12**, 516–527 (2018).
4. L. Robledo *et al.*, *Nature* **477**, 574–578 (2011).
5. K. D. Jöns *et al.*, *Phys. Rev. B* **96**, 075430 (2017).
6. H. Bernien *et al.*, *Nature* **497**, 86–90 (2013).
7. D. Bluvstein, Z. Zhang, A. C. B. Jayich, *Phys. Rev. Lett.* **122**, 076101 (2019).
8. B. Kambs, C. Becher, *New J. Phys.* **20**, 115003 (2018).
9. L. C. Bassett, F. J. Heremans, C. G. Yale, B. B. Buckley, D. D. Awschalom, *Phys. Rev. Lett.* **107**, 266403 (2011).
10. C. F. de las Casas *et al.*, *Appl. Phys. Lett.* **111**, 262403 (2017).
11. W. Pfaff *et al.*, *Science* **345**, 532–535 (2014).
12. V. M. Acosta *et al.*, *Phys. Rev. Lett.* **108**, 206401 (2012).
13. Y. Chu *et al.*, *Nano Lett.* **14**, 1982–1986 (2014).
14. J. Wolters, N. Sadzak, A. W. Schell, T. Schröder, O. Benson, *Phys. Rev. Lett.* **110**, 027401 (2013).

15. T. Murai *et al*., *Appl. Phys. Lett.* **112**, 111903 (2018).
16. S. B. van Dam *et al*., *Phys. Rev. B* **99**, 161203 (2019).
17. K. Beha, A. Batalov, N. B. Manson, R. Bratschitsch, A. Leitenstorfer, *Phys. Rev. Lett.* **109**, 097404 (2012).
18. G. Wolfowicz *et al*., *Nat. Commun.* **8**, 1876 (2017).
19. B. J. Shields, Q. P. Unterreithmeier, N. P. de Leon, H. Park, M. D. Lukin, *Phys. Rev. Lett.* **114**, 136402 (2015).
20. P. Siyushev *et al*., *Science* **363**, 728–731 (2019).
21. W. F. Koehl, B. B. Buckley, F. J. Heremans, G. Calusine, D. D. Awschalom, *Nature* **479**, 84–87 (2011).
22. D. J. Christle *et al*., *Nat. Mater.* **14**, 160–163 (2015).
23. P. V. Klimov, A. L. Falk, D. J. Christle, V. V. Dobrovitski, D. D. Awschalom, *Sci. Adv.* **1**, e1501015 (2015).
24. D. J. Christle *et al*., *Phys. Rev. X* **7**, 021046 (2017).
25. M. Kim *et al*., *Phys. Rev. Lett.* **115**, 087602 (2015).
26. M. S. Grinolds *et al*., *Nat. Nanotechnol.* **9**, 279–284 (2014).
27. M. Pfender *et al*., *Nano Lett.* **17**, 5931–5937 (2017).
28. M. Widmann *et al*., *Appl. Phys. Lett.* **112**, 231103 (2018).
29. P. V. Klimov, A. L. Falk, B. B. Buckley, D. D. Awschalom, *Phys. Rev. Lett.* **112**, 087601 (2014).
30. M. W. Doherty *et al*., *Phys. Rev. X* **6**, 041035 (2016).
31. M. Niethammer *et al*., Coherent electrical readout of defect spins in 4H-SiC by photo-ionization at ambient conditions. arXiv:1903.12236 [cond-mat.mes-hall] (28 March 2019).
32. See the supplementary materials.
33. M. Widmann *et al*., *Nat. Mater.* **14**, 164–168 (2015).
34. N. T. Son *et al*., *Phys. Rev. Lett.* **96**, 055501 (2006).
35. A. Beste, D. E. Taylor, D. A. Golter, C. W. Lai, *Phys. Rev. B* **98**, 214107 (2018).
36. M. Shimizu *et al*., *Appl. Phys. Express* **11**, 033004 (2018).
37. K. Ohno *et al*., *Appl. Phys. Lett.* **101**, 082413 (2012).
38. J. R. Maze *et al*., *New J. Phys.* **13**, 025025 (2011).
39. S. J. Whiteley *et al*., *Nat. Phys.* **15**, 490–495 (2019).
40. K. C. Miao *et al*., *Sci. Adv.* **5**, eaay0527 (2019).
41. J. Forneris *et al*., *Phys. Rev. Appl.* **10**, 014024 (2018).
42. S. Wengerowsky, S. K. Joshi, F. Steinlechner, H. Hübel, R. Ursin, *Nature* **564**, 225–228 (2018).
43. D. A. Broadway *et al*., *Nat. Electron.* **1**, 502–507 (2018).
44. A. N. Vamivakas *et al*., *Phys. Rev. Lett.* **107**, 166802 (2011).
45. F. Dolde *et al*., *Nat. Phys.* **7**, 459–463 (2011).
46. G. Wolfowicz, S. J. Whiteley, D. D. Awschalom, *Proc. Natl. Acad. Sci. U.S.A.* **115**, 7879–7883 (2018).
47. N. R. Jungwirth *et al*., *Nano Lett.* **16**, 6052–6057 (2016).
48. S. O. Hruszkewycz *et al*., *Phys. Rev. Mater.* **2**, 086001 (2018).
49. H. Thyrrestrup *et al*., *Nano Lett.* **18**, 1801–1806 (2018).
50. M. C. Löbl *et al*., *Phys. Rev. B* **96**, 165440 (2017).
51. C. Chakraborty, L. Kinnischtzke, K. M. Goodfellow, R. Beams, A. N. Vamivakas, *Nat. Nanotechnol.* **10**, 507–511 (2015).
52. C. Schreyvogel, V. Polyakov, R. Wunderlich, J. Meijer, C. E. Nebel, *Sci. Rep.* **5**, 12160 (2015).
53. H. Kato *et al*., *Appl. Phys. Lett.* **102**, 151101 (2013).
54. F. J. Heremans, G. D. Fuchs, C. F. Wang, R. Hanson, D. D. Awschalom, *Appl. Phys. Lett.* **94**, 152102 (2009).
55. D. A. Golter, C. W. Lai, *Sci. Rep.* **7**, 13406 (2017).
56. B. Magnusson *et al*., *Phys. Rev. B* **98**, 195202 (2018).
57. N. Aslam, G. Waldherr, P. Neumann, F. Jelezko, J. Wrachtrup, *New J. Phys.* **15**, 013064 (2013).
58. M. Bockstedte, F. Schütz, T. Garratt, V. Ivády, A. Gali, *npj Quant. Mater.* **3**, 31 (2018).
59. P. Siyushev *et al*., *Phys. Rev. Lett.* **110**, 167402 (2013).
60. A. V. Kuhlmann *et al*., *Nat. Phys.* **9**, 570–575 (2013).
61. M. Widmann *et al*., *Nano Lett.* **19**, 7173–7180 (2019).
62. C. P. Anderson *et al*., Dataset for: Electrical and optical control of single spins integrated in scalable semiconductor devices, Zenodo (2019); https://doi.org/10.5281/zenodo.3523353.

ACKNOWLEDGMENTS

We thank E. O. Glen, S. Bayliss, D. J. Christle, P. V. Klimov, and P. J. Duda for helpful experimental suggestions and assistance and A. Gali, G. Galli, M. E. Flatté, D. R. Candido, and B. Magnusson for insightful discussions and theoretical understanding. Careful reading by F. J. Heremans supported manuscript preparation. We thank *Quantum Opus* for their assistance with SNSPDs.

Funding: This work made use of the UChicago MRSEC (NSF DMR-1420709) and Pritzker Nanofabrication Facility, which receives support from the SHyNE, a node of the NSF's National Nanotechnology Coordinated Infrastructure (NSF ECCS-1542205). C.P.A., A.B., K.C.M., G.W., P.J.M., A.L.C., and D.D.A. were supported by AFOSR FA9550-14-1-0231 and FA9550-15-1-0029, DARPA D18AC00015KK1932, NSF EFRI EFMA-1641099, and ONR N00014-17-1-3026. C.P.A. was supported by the Department of Defense through the NDSEG Program. T.O. was supported by KAKENHI (17H01056 and 18H03770). J.U.H was supported by the Swedish Energy Agency (43611-1). N.T.S. was supported by the Swedish Research Council (VR 2016-04068) and the Carl Tryggers Stiftelse för Vetenskaplig Forskning (CTS 15:339). J.U.H. and N.T.S. were also supported by the Knut and Alice Wallenberg Foundation (KAW 2018.0071). **Author contributions:** C.P.A and A.B. conceived the experiments, fabricated the devices, performed the measurements, and analyzed the data. A.B. and K.C.M developed the experimental setup. A.L.C. assisted in device fabrication. H.A. and T.O. performed the electron irradiation. J.U.H. and N.T.S. assisted in growth and sample preparation of initial test devices used before the commercial samples. G.W. and P.J.M. measured initial devices. D.D.A. advised on all efforts. All authors contributed to the data analysis and manuscript preparation. **Competing interests:** A patent application has been filed relating to this work. P.J.M. is a paid consultant to ARCH Venture Partners. **Data and materials availability:** The data can be accessed at Zenodo (*62*).

SUPPLEMENTARY MATERIALS

6 May 2019; accepted 5 November 2019
10.1126/science.aax9406

Electrical and optical control of single spins integrated in scalable semiconductor devices

Christopher P. Anderson, Alexandre Bourassa, Kevin C. Miao, Gary Wolfowicz, Peter J. Mintun, Alexander L. Crook, Hiroshi Abe, Jawad Ul Hassan, Nguyen T. Son, Takeshi Ohshima and David D. Awschalom

Science **366** (6470), 1225-1230.
DOI: 10.1126/science.aax9406

Divacancies in a diode

Solid-state defects hold great promise as the building blocks for quantum computers. Most research has focused on defects in diamond, which are difficult to integrate with existing semiconductor technologies. An alternative two-vacancy neutral defect in silicon carbide (SiC) has a long coherence time but suffers from broad optical linewidths and charge instability. Anderson *et al.* fabricated these defects in a diode made out of commercially available SiC. Reverse voltage created large electric fields within the diode, tuning the frequencies of the defect's transitions by hundreds of gigahertz. The electric fields also caused charge depletion, leading to a dramatic narrowing of the transitions. The technique should be readily generalizable to other quantum defects.

Science, this issue p. 1225